Kinetic energy release in unimolecular reactions of spherical clusters

K. Hansen [1]

Dept. of Experimental Physics, Gothenburg University and Chalmers University of Technology, SE-41296 Gothenburg, Sweden

Abstract

The distribution of translational kinetic energy releases in unimolecular reactions is discussed with special emphasis on the distributions for reactions with no reverse activation barrier and the role of long range spherical potentials between the fragments. The distributions are calculated with detailed balance. Angular momentum conservation is included, and total rate constants are given.

Key words: Kinetic energy release, unimolecular, detailed balance, clusters

PACS: 36.40.Qv, 36.40.Wa

Email address: klavs@fy.chalmers.se (K. Hansen).

URL: http://fy.chalmers.se/ klavs/ (K. Hansen).

[1] Dept. of Experimental Physics, Gothenburg University and Chalmers University of Technology, SE-41296 Gothenburg, Sweden

Phone +46 (0)31 772 3233, FAX +46 (0)31 772 3496

1 Introduction

The determination of thermal properties and binding energies of gas phase clusters is an important component in the characterization of these species. Any experimentally accessible quantity which provides information of this is therefore of great importance. One of the most important is the kinetic energy of the fragments in unimolecular reactions. These energies can be measured relatively easily and yield an absolute value of the average kinetic energies released and often provide the entire distribution of kinetic energies [1–3]. The distributions are measures of the statistical weight with which each individual kinetic energy is emitted and may be converted into an effective temperature. The conversion from kinetic energy release distributions (KERD) to a temperature depends on details of the system, i.e. there are several system-specific parameters beyond the temperature which determine the KERD. The purpose of this letter is to derive this dependence when the long range interaction between the two fragments is attractive and spherically symmetric.

Several theoretical studies on KERDs exist. Pechukas and Light have presented an impressively argued case for detailed balance results on the unimolecular decay of trimers [4]. Unfortunately the product of this reaction, a dimer, is about as far from spherical shape as one can imagine, and we will therefore not use these results.

Klots has derived results pertaining to the motion of particles in a spherically symmetric potential. In [5] kinetic energy release in a Langevin potential (see Eq.(5)) was examined for point particles. In [6] the analysis was extended to a point charge and a polarizable particle and a cutoff distance was derived

from the neutral particle. However, for most cluster applications the result will seriously underestimate the hard sphere cross section and effect adversely calculated KERDs. Another difference to the present work is that velocity bias in the flux, required by detailed balance [7], was not included.

Chesnavich and Bowers have derived a number of results on angular momentum related level densities in the classical limit [8]. The results should permit classically exact angular momentum conservation in calculations of unimolecular rate constants for a large group of molecular shapes. This is potentially useful for the present work but, as it turns out, they are not needed because a direct calculation is very simple.

The calculation presented here uses the detailed balance approach. It has been argued, based on numerical simulations [10], that this does not give an accurate quantitative description of rate constants. The claim originates in a comparison with the formula in [11], which is the detailed balance result [12,13], but restricted to a geometric cross section and a classical harmonic oscillator level density. Since at least the latter assumption is contradicted by the authors' own simulations, the claim appears unsubstantiated.

The paper is divided into four parts. First the detailed balance rate constant without conservation of angular momentum is presented, with special emphasis on the KERD. Next the capture cross section is derived for spherical symmetric attractive potentials with some reasonably general properties. Then the angular momentum conservation is applied and the necessary modifications to the rate constants introduced. Finally, a numerical example demonstrates some dangers in the analysis of experimental data.

2 General statistical theory

The detailed balance rate constant, specified with respect to the kinetic energy of the outgoing channel, is given by [7,12]

$$k(E;\varepsilon) = \frac{g\mu}{\pi^2\hbar^3}\sigma(\varepsilon)\varepsilon\frac{\rho_d(E-D-\varepsilon)}{\rho_p(E)}, \tag{1}$$

where E is the excitation energy of the parent cluster, g is the electronic degeneracy of the evaporated atom, μ is the reduced mass, ε is the kinetic energy release, i.e. the sum of the translational kinetic energy of the two fragments, D is the dissociation energy, $\sigma(\varepsilon)$ is the cross section for capture of the fragment in the inverse process, and ρ_d, ρ_p is the level density of the daughter and the parent cluster.

The level density of the product cluster can be factored as [14];

$$\rho_d(E-D-\varepsilon) \approx \rho_d(E-D)exp(-\varepsilon/T_m), \tag{2}$$

where the microcanonical temperature T_m is defined as

$$T_m^{-1} \equiv \frac{d\ln(\rho_d(E-D))}{dE}. \tag{3}$$

The two equations follow from of a simple Taylor expansion of the logarithm of the level density. The correction is on the order of $(\varepsilon/T_m)^2/(2C_v)$, where C_v is the heat capacity of the daughter cluster (in units of k_B) and will be ignored in the following. The total kinetic energy distribution is therefore

$$k(E;\varepsilon) = \frac{g\mu}{\pi^2\hbar^3}\sigma(\varepsilon)\varepsilon exp(-\varepsilon/T_m)\frac{\rho_d(E-D)}{\rho_p(E)}. \tag{4}$$

3 Cross section

We now turn to the cross section. It is calculated for a classical motion in a long range potential and sticking when the daughter cluster and the small fragment are within a certain distance, the capture radius, denoted r_0. The sticking does not have to be unity but will be assumed independent of ε and the angular momentum of the daughter cluster. We will assume that the potential has the form

$$V(r) = -\frac{\alpha e^2}{2r^4} - \sum_{n=0}^{\infty} \frac{C_{6+2n}}{r^{6+2n}}, \tag{5}$$

where the first term is the potential due to the polarizability of the neutral fragment in an ion-neutral system. It may also, with minor modifications, apply to thermal electron emission from anions (see [15]). The units are gaussian. The polarization energy converts to $14.4eV\mathring{A}\alpha/2r^4$, with α and r in $\mathring{A}^3$ and $\mathring{A}$, respectively. Terms beyond the polarizability interaction can be both relevant and measured [16].

The simplest picture is found when $r^2V(r)$ is negative, has a positive slope and a negative curvature. This covers all cases with non-positive coefficients in the expansion of the potential in terms of $1/r^2$ (except the trivial case where all coefficients are zero). Angular momentum conservation, $L = v_0 b\mu = constant$, where b is the impact parameter, v_0 the relative speed of the asymptotically separated particles, and μ is the reduced mass of the two fragments, gives, together with energy conservation and $\varepsilon = \mu v_0^2/2$:

$$\varepsilon = V(r) + \frac{\mu \dot{r}^2}{2} + \varepsilon \frac{b^2}{r^2}. \tag{6}$$

At the turning point of the radial motion, if it exists, $\dot{r} = 0$. For this point the equation reduces to

$$V(r) + \varepsilon\frac{b^2}{r^2} - \varepsilon = 0 \Rightarrow \frac{r^2 V(r)}{\varepsilon} = r^2 - b^2. \tag{7}$$

The solution to the equation can be illustrated graphically. The two sides of this equation plotted *vs* r^2 give a straight line with slope 1 and a negative function with positive slope and a negative curvature (see Fig.(1)). These properties derive from the assumptions of the potential. Initially, we will consider point particles and need therefore only calculate the turning points. They are given by the intersection of the left and right hand sides of Eq.(7). For a fixed energy it has solutions for values of b^2 larger than or equal to the values where the straight line is tangential to the $r^2V(r)$ curve. The two conditions that the curves are tangential are Eq.(7) and its derivative;

$$\frac{d}{dr^2}\left(\frac{r^2V(r)}{\varepsilon}\right)|_{r_c} = \frac{d}{dr^2}\left(r^2 - b^2\right)|_{r_c} = 1. \tag{8}$$

The negative curvature of $r^2V(r)$ ensures that there is precisely one real solution for b^2 to these two equations. A little algebra gives the value of the critical impact parameter b_c and hence the capture cross section;

$$\sigma_{cap} = \pi b_c^2 = \pi\left(r_c^2 + \frac{1}{\varepsilon}\left(\frac{\alpha e^2}{2r_c^2} + \sum_{n=0}^{\infty}\frac{C_{6+2n}}{r_c^{6+2n}}\right)\right), \tag{9}$$

where r_c is the root of:

$$\frac{\alpha e^2}{2r_c^4} + \sum_{n=0}^{\infty}(n+2)\frac{C_{6+2n}}{r_c^{6+2n}} - \varepsilon = 0. \tag{10}$$

Physically, r_c is the smallest turning point (in the inward motion) for the energy ε and the given potential. In the special case when $C_{6+2n} = 0 (n > 2)$,

this is at most a quartic equation in r_c^{-2} and can be solved analytically. When only the term with α is non-zero, the cross section reduces correctly to the Langevin cross section,

$$\sigma_{cap} = \pi \left(\frac{2\alpha e^2}{\varepsilon} \right)^{1/2}. \tag{11}$$

Let's now add the finite capture radius, r_0, to the problem. From the equation for r_c above and the properties of the potential it is easy to see that r_c increases monotonously when ε decreases. Also the derivative $db_c^2/d\varepsilon$ is negative, which can be verified by differentiation of the cross section and using the equation which determines r_c. We therefore have that the cross section is given by Eqs.(9) and (10) when

$$\varepsilon \leq \frac{\alpha e^2}{2r_0^4} + \sum_{n=0}^{\infty} (n+2) \frac{C_{6+2n}}{r_0^{6+2n}}. \tag{12}$$

Note that this energy is in general not the potential energy at r_0. For energies exceeding this value, we have two turning points in the radial motion, of which the smallest, unphysical one, is inside the cluster. The cross section corresponds to the largest turning point and can be found by reference to Fig.(1), and with Eq.(7) evaluated at the capture radius, $r = r_0$. Thus

$$\sigma_{cap} = \pi r_0^2 \left(1 - \frac{V(r_0)}{\varepsilon} \right), \quad \varepsilon \geq \frac{\alpha e^2}{2r_0^4} + \sum_{n=0}^{\infty} (n+2) \frac{C_{6+2n}}{r_0^{6+2n}}. \tag{13}$$

The interaction energy is negative, and hence the cross section is larger than geometric. The increase is due to the deflection of the small fragment in the attractive potential and the resulting enhanced chance to coalesce with the cluster. At high energies this effect reduces in importance, as witnessed by the $1/\varepsilon$ dependence of the correction to the geometric cross section.

The cross section is thus a combination of two different functional forms, one which is valid for small energies and which is a generalized Langevin cross section, and another part, valid at high energies, which is a modified geometric potential. The cross section is continuous across the critical energy which separates these two regimes.

4 Angular momentum conservation

The above treatment only includes angular momentum conservation in the orbital motion. We will restrict the treatment here to daughter clusters which are spherical top molecules. This is partly motivated by the assumption of spherical potentials in this work, and partly by the general tendency for clusters to have a spherical shape. Interestingly, the analysis does not seem to require any symmetry of the parent. The angular momentum will be treated as a classical variable, which is generally justified by the magnitude of the angular momentum quantum numbers involved, except possibly for cases of electron emission from cluster anions. The small fragment will be assumed to have no appreciable internal angular momentum.

The magnitude of the orbital angular momentum in the relative motion of the small fragment and the daughter cluster is $L_o = b(2\mu\varepsilon)^{1/2}$. We can therefore write the cross section as

$$\sigma(\varepsilon) = \pi \int_0^{b_c} db 2b = 2\pi \int_0^{L_{o,max}} dL_o \frac{L_o}{2\mu\varepsilon}, \tag{14}$$

where $b_c(\varepsilon) = \sqrt{\sigma(\varepsilon)/\pi}$, and $L_{o,max} = b_c(2\mu\varepsilon)^{1/2}$. If we specify the direction of

L_o in spherical polar coordinates we have

$$\sigma(\varepsilon) = \frac{\pi}{4\pi} \int_0^{2\pi} d\phi \int_0^{\pi} d\theta sin(\theta) \int_0^{b_c(2\mu\varepsilon)^{1/2}} dL_o \frac{L_o}{\mu\varepsilon}, \tag{15}$$

where the 4π is the normalization of the angular integration. Eq.(15) will be used to rewrite Eq.(1). The argument of the daughter level density is also changed in order to conserve energy. This gives

$$k(E;\varepsilon) = \frac{g\mu}{\pi^2\hbar^3}\frac{1}{4}\int_0^{2\pi}\int_0^{\pi} d\phi d\theta sin(\theta) \int_0^{b_c(2\mu\varepsilon)^{1/2}} dL_o \frac{L_o}{\mu\varepsilon}\varepsilon \frac{\rho_d(E - D - \varepsilon + \varepsilon_{p,r} - \varepsilon_{d,r})}{\rho_p(E)}, \tag{16}$$

where $\varepsilon_{p,r} = L^2/2I_p$ is the rotational energy of the parent with angular momentum $\overline{L}$ and a properly averaged moment of inertia I_p of the parent, and $\varepsilon_{d,r} = (\overline{L} - \overline{L_o})^2/2I_d$ is the rotational energy of the daughter. Choosing $\theta = 0$ along the direction of $\overline{L}$ gives us

$$\varepsilon_{d,r} = \frac{L^2 + L_o^2 - 2LL_o cos(\theta)}{2I_d}. \tag{17}$$

With the substitution $x = cos(\theta)$ and integrating over ϕ we have

$$k(E;\varepsilon) = \frac{g\mu}{\pi^2\hbar^3}\frac{\pi}{2\mu\rho_p(E)}\int_{-1}^{1} dx \int_0^{b_c(2\mu\varepsilon)^{1/2}} dL_o \rho_d(E'), \tag{18}$$

where $E' \equiv E - D - \varepsilon + \frac{L^2}{2I_p} - \frac{L^2 + L_o^2 - 2LL_o x}{2I_d}$.

This expression cannot be simplified without some restrictions on the magnitude of the involved rotational energies. We will argue that simplifications are often possible. Unless the parent cluster has a rotational energy considerable higher than that corresponding to the (microcanonical) emission temperature in Eq.(3), the term $L^2/2I_p$ will be of the same magnitude as or smaller than

a typical value of ε. The difference $L^2(1/2I_p - 1/2I_d)$ will therefore also be small.

The term $L_o^2/2I_d$ will be reduced compared with typical values of ε with the factor $\mu b_c^2/I_d$ and hence will not be large. The same arguments apply to the last term in the level density.

We can then expand the logarithm of the level density in analogy to Eq.(2). After integration over x we have

$$k(E;\varepsilon) = \frac{g\mu}{\pi^2\hbar^3}\frac{\rho_d(E-D)}{\rho_p(E)}e^{-\varepsilon/T}\frac{\pi I_d T}{2\mu L}e^{\frac{L^2}{T}\left(\frac{1}{2I_p}-\frac{1}{2I_d}\right)}\times \tag{19}$$

$$\int_0^{b_c(2\mu\varepsilon)^{1/2}} dL_o \left[e^{-\frac{L_o^2}{2I_dT}+\frac{2LL_o}{2I_dT}} - e^{-\frac{L_o^2}{2I_dT}-\frac{2LL_o}{2I_dT}}\right]$$

The integral can be expressed in terms of the error function as

$$k(E;\varepsilon) = \frac{g\mu}{\pi^2\hbar^3}\frac{\rho_d(E-D)}{\rho_p(E)}e^{-\varepsilon/T}e^{\frac{L^2}{2I_pT}}\frac{(2\pi I_dT)^{3/2}}{8\mu L}\times \tag{20}$$

$$\left[erf\left(\frac{b_c(2\mu\varepsilon)^{1/2}-L}{(2I_dT)^{1/2}}\right) - erf\left(\frac{b_c(2\mu\varepsilon)^{1/2}+L}{(2I_dT)^{1/2}}\right) + 2erf\left(\frac{L}{(2I_dT)^{1/2}}\right)\right]$$

Alternatively, one may expand the integrand in Eq.(19) and perform integration term by term to get, to next-to-leading order in $1/2I_dT$:

$$k(E;\varepsilon) = \frac{g\mu}{\pi^2\hbar^3}\frac{\rho_d(E-D)}{\rho_p(E)}\varepsilon e^{-\varepsilon/T}\sigma(\varepsilon)e^{\frac{L^2}{T}\left(\frac{1}{2I_p}-\frac{1}{2I_d}\right)}\left(1+\frac{\sigma(\varepsilon)\mu\varepsilon}{2\pi I_dT}\left(\frac{L^2}{12I_dT}-1\right)\right). \tag{21}$$

The correction to the rate constant of Eq.(4) consists of the two last factors.

Together with the equations which determine the cross sections, Eqs.(18,21) describe the rate constants and the kinetic energy releases during evaporation of atoms with a spherical top product cluster for no reverse activation barrier,

when the small and large fragments interact through spherically symmetrical potentials with the properties specified above.

5 Examples

As an illustration of the results we have calculated the kinetic energy releases for the case where α is the only non-vanishing coefficient in the potential. Most of the changes relative to e.g. a simple dark sphere cross section come from the kinetic energy dependence of the cross section, and in order to get a clear picture of this effect, the corrections from angular momentum conservation will be set to zero.

Combining the low- and high energy cross sections, Eqs.(9,13), and scaling with the temperature, one arrives at the kinetic energy distributions

$$P(\varepsilon) \propto \left(\frac{\varepsilon}{T} + \frac{\alpha e^2}{2r_0^4 T}\right) exp(-\varepsilon/T), \qquad \varepsilon \geq \frac{\alpha e^2}{2r_0^4} \tag{22}$$

$$P(\varepsilon) \propto 2\left(\frac{\alpha e^2}{2r_0^4 T}\right)^{1/2} \left(\frac{\varepsilon}{T}\right)^{1/2} exp(-\varepsilon/T), \qquad \varepsilon \leq \frac{\alpha e^2}{2r_0^4},$$

where the constant of proportionality is the same. Curves for different values of $\alpha e^2/2r_0^2 T$ are shown in Fig.(2).

Ideally the temperature in these curves can be fitted from the high energy tail of the distribution, but in practice this will often be impossible for reasons of statistics. As an alternative it has been suggested to use a so-called modelfree approach, where the distributions are fitted with the function $P(\varepsilon) \propto \varepsilon^l exp(-\varepsilon/T)$, where both l and T are fit parameters. It is therefore interesting to examine how well this fit formula is able to represent the simple case

simulated here. In all cases shown, the calculated curves can be fitted quite well with this formula. Problems arise in the value of the fitted parameters, however. The introduction of l is *ad hoc* and cannot be assigned much physical significance. More interesting is the temperature derived from the fit. Fig.(3) shows the ratio of fitted temperatures to the ones used to calculate the fitted curves, i.e. the one used as input in Eq.(22). It is seen that only in the two extreme cases of no polarizability and extremely strong polarizability does the 'modelfree' approach represent the curves correctly. It is expected that these two limits give correct answers since they correspond to a geometric cross section and a Langevin cross section, respectively, but at all other values the fitted temperature is too high, by as much as 20%.

To further illustrate the relevance of this calculation, we have calculated the value of the parameter on the abscissa for a few clusters, $Ar_{10}^+, Ar_{100}^+, Na_{10}^+$ and Na_{100}^+. The temperature was set to 30K for Ar and 300 K for Na, and the contact radius calculated as $r_0 = r_1((n-1)^{1/3}+1)$, where r_1 is the atomic radius derived from the bulk value of the atomic volume of $4\pi r_1^3/3$. The values of $e^2\alpha/2r_0^4$ were 2.8 for Ar_{10}^+, 0.25 for Ar_{100}^+, 3.8 for Na_{10}^+ and 0.34 for Na_{100}^+. The fact that these values depend strongly on the capture radius notwithstanding, the numerical examples amply illustrate the importance of a correct treatment of the polarizability interaction in the analysis.

A more intensely studied kinetic energy release, that of C_2 emission from fullerenes, can strictly speaking not be analysed with the results here, because the C_2 carries a finite internal angular momentum. Since we expect relatively minor corrections to the KERDs from this, it is still interesting to estimate $\alpha e^2/2r^4T$ for this system. With a value of 2.8Å^3 for α [17], and a daughter temperature of 3500K, one gets $\alpha e^2/2r^4T = 0.45,\ 0.26$ and 0.11 for a capture

radius of $3.5, 4$ and $5\mathring{A}$, respectively. This calculation does not include the unknown but possibly relevant higher order terms in Eq.(5). It nevertheless suggests that the explanation that the KERDs observed in [17] are fitted so well with a Langevin type cross section, is the result of an induced dipole interaction. Conversely, if we assume a contact radius of 4Å and l-value between 0.45 and 0.55, the polarizability is limited to $\alpha \geq 3.2\mathring{A}^3$. For contact radii of 3.5 and 5Å, the limits are 1.9 and 7.9Å^3, respectively. These limits seem close enough to realistic values to warrant further analysis of experimental data.

6 Acknowledgements

Comments on the manuscript from K.Mehlig and O.Echt are gratefully acknowledged.

References

[1] J.Laskin and C.Lifshitz, *J.Mass Spectrom.* **36** (2001) 459

[2] S.Matt et al., *Eur. Mass Spectrom.* **5** (1999) 477

[3] S.Tomita, H.Lebius, A.Brenac, F.Chandezon, and B.A.Huber, *Phys.Rev. A* **65** (2002) 053201

[4] P.Pechukas and J.C.Light, *J.Chem.Phys.* (1965) 3281

[5] C.E.Klots, *J.Chem.Phys.* **64** (1976) 4269

[6] C.E.Klots, *J.Chem.Phys.* **100** (1994) 1035

[7] K.Hansen, *Philos. Mag. B* **79** (1999) 1413

[8] W.J.Chesnavich and M.T.Bowers, *J.Chem.Phys.* **66** (1977) 2306

[9] L.D.Landau and E.M.Lifshitz, Statistical Physics, Part 1, 3.rd edition, Pergamon Press, Oxford (1986).

[10] S.Weerasinghe and F.G.Amar, *J.Chem.Phys.* **98** (1993) 4967

[11] P. Engelking, *J. Chem. Phys.* **87** (1987) 936

[12] V. Weisskopf, *Phys. Rev.* **52** (1937) 259

[13] P.Fröbrich and R.Lipperheide, Theory of Nuclear Reactions, Oxford Studies in Nuclear Physics 18, Oxford Science Publications (1996).

[14] S. Frauendorf, *Z. Phys. D* **35** (1995) 191

[15] V.V.Kresin and C.Guet, *Philos. Mag. B* **79** (1999) 1401

[16] V.V.Kresin et al., *J.Chem.Phys.* **108** (1998) 6660 *J.Chem.Phys.* **118** (2003) 7313

[17] K. Gluch et al., On the Kinetic Energy Release Distribution for C_2 Evaporation from Fullerene Ions, *Chem. Phys. Lett.*, to appear.

7 Figure captions

Fig.1

Schematics of the left and right hand side of Eq.(7). The high energy curve, for ε_1, corresponds to the modified geometric cross section in Eq.(13) with the value πb_1^2. The low energy curve, with ε_2, corresponds to the cross section given by Eq.(9) and cross section πb_2^2. The capture radius r_0 is indicated by the dotted vertical line.

Fig.2

Kinetic energy distributions calculated with the Eqs.(22) in their respective energy regions of validity for six different values of the strength of the polarizability interaction.

Fig.3

Parameters of the kinetic energy distributions shown in Fig.2, fitted with the so-called modelfree approach, $P(\varepsilon) \propto \varepsilon^l exp(-\varepsilon/T)$. For a range of values of the interaction strength this formula seriously overestimates the temperature.

Fig.1, K.Hansen, Kinetic energy..

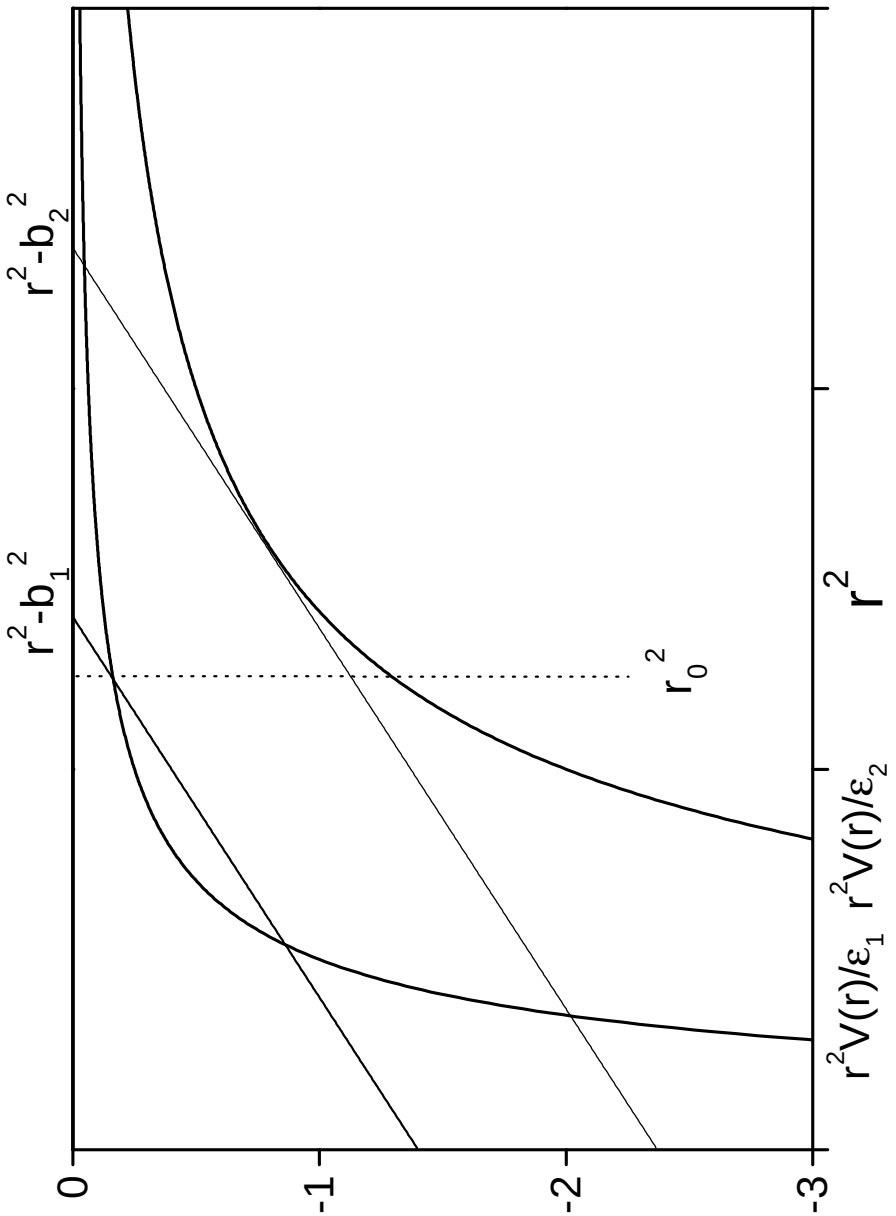

Fig.2, K.Hansen, Kinetic energy..

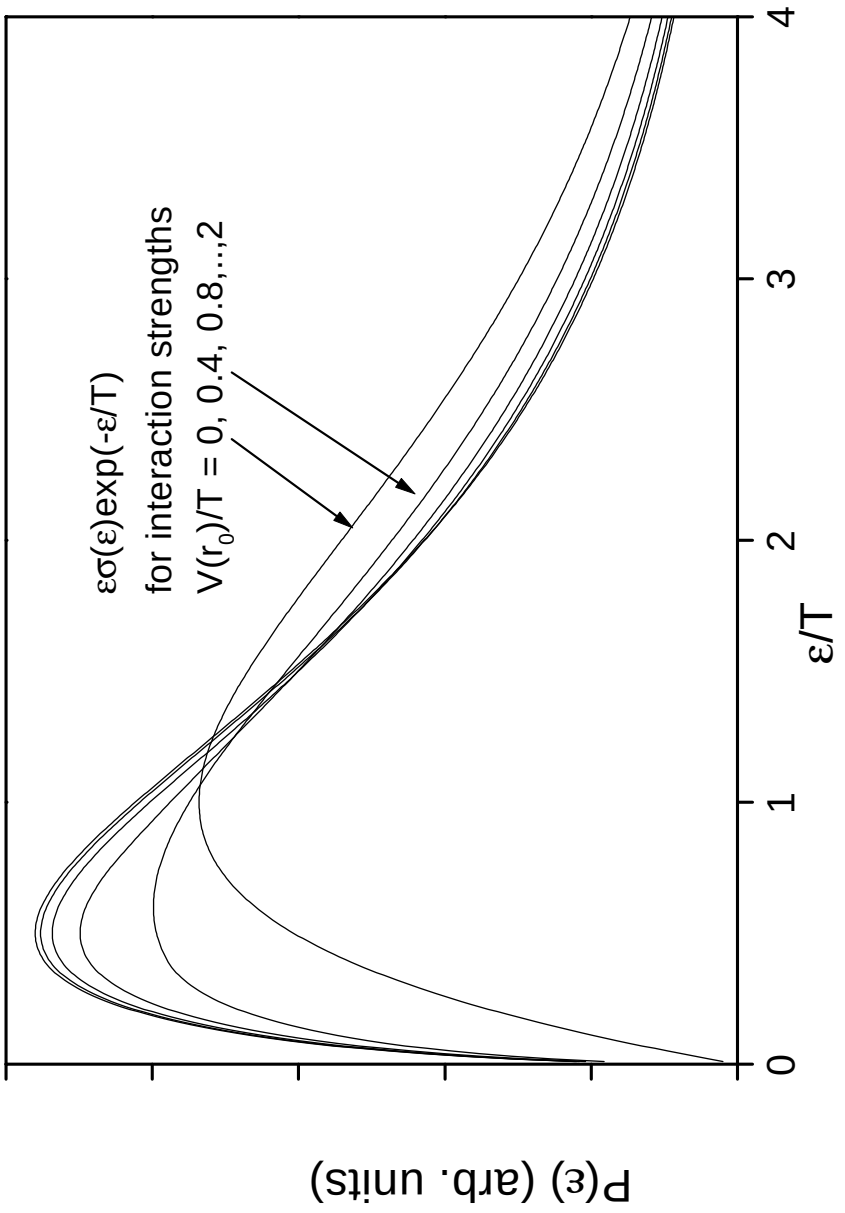

Fig.3, K.Hansen, Kinetic energy..